CBPF-NF-008/82

SELF-CONSISTENT EMBEDDED-CLUSTER CALCULATIONS OF THE ELECTRONIC STRUCTURE OF ALKALINE EARTH FLUORIDES IN THE HARTREE-FOCK-SLATER APPROXIMATION

by

Nelson C. Amaral[1], B. Maffeo[2]
and Diana Guenzburger

Centro Brasileiro de Pesquisas Físicas - CBPF/CNPq
Rua Xavier Sigaud, 150
22290 - Rio de Janeiro - RJ - BRASIL

[1]Departamento de Física, Universidade Federal de Goiás
CP. 597 - Goiania 74000 - Goiás - BRASIL

[2]Sociedade Brasileira de Física
Rio de Janeiro - RJ - BRASIL

ABSTRACT

Molecular orbitals calculations were performed for clusters representing the CaF_2, SrF_2 and BaF_2 ionic crystals. The discrete variational method was employed, with the Xα approximation for the exchange interaction; a detailed investigation of different models for embedding the clusters in the solids led to a realistic description of the effect of the neighbour ions in the infinite crystal. The results obtained were used to interpret optical and photoelectron data reported in the literature. In the case of CaF_2, comparisons were made with existing band structure calculations.

I. INTRODUCTION

The alkaline earth fluorides CaF_2, SrF_2 and BaF_2 are ionic crystals presenting the fluorite structure, and are insulators characterized by a large energy gap between the valence states and the empty conduction band. Optical properties were measured in the UV region[1-5]; ultraviolet and X-ray photoelectron spectroscopy studies were also reported[6,7], as well as characteristic electron energy losses[8-10]. The electronic spectra of these crystals are complex, presenting structure due to interband and excitonic transitions.

Other motivations for the increasing interest in these compounds in recent years are their utilization as window materials in optical experiments[11] and the construction of crystal laser systems of rare earth ions in alkaline earth fluoride hosts[12]. Finally, these compounds find extensive use as host materials for investigating optical and magnetic properties of impurity ions (in particular, rare earth ions[13]), vacancies and other defects[14].

We were interested in a theoretical investigation of the fundamental electronic properties of CaF_2, SrF_2 and BaF_2 which is needed for a better understanding of the experimental data. For this purpose, we employed a cluster model to calculate the electronic structure of these compounds; in this model, translation symmetry is not considered and only a limited number of atoms is included. Cluster models have been employed in investigating electronic properties of different periodic systems[15-18]; they are obviously more limited than complete band structure calculations, but they also provide a great deal of qualitative and quantitative information, having the advantage of a much smaller computational effort. In the present case, band calculations are rather complicated due to

the presence of three atoms per unit cell, and were reported only for CaF_2[19-21]. Our purpose was then to make cluster calculations for this compound, and compare with both the experimental data and band calculations; in addition, we also obtained the electronic structure of SrF_2 and BaF_2, for which the experimental data is also rich but no band calculations are available. The present paper is organized in the following manner: in section II is described the self-consistent Hartree - Fock - Slater(HFS) method that was employed in calculating the one-electron energies and eigenfunctions for the cluster; special attention will be given to the external environment of the cluster, since this has to be adequately described for a meaningful simulation of the infinite cristal. In section III we present our results and discuss them together with the experimental data. For CaF_2, we also make comparisons with the band structure calculations reported. In section IV we draw our conclusions.

II. THEORETICAL MODEL

The one-electron description of a crystalline solid may be achieved in two manners. The first preserves the translational symmetry of the crystal, associating Bloch functions to the electrons. An alternative to this procedure which is by far less laborious computationally is to consider a cluster of atoms taken from the crystal and perform Molecular Orbital (MO) calculations to obtain the one-electron energies and eigenfunctions. The environment of the cluster in the solid is taken into account in an approximate

manner by the inclusion of an appropriate field in which the cluster is embedded. One must have in mind the limitations of this second model, which does not take into account the periodicity of the crystal; however, it may be used to understand many properties and, at the present stage, is in most cases the only model applicable to impurities, localized excitations, vacancies and amorfous solids.

In this section the description of the calculations will be devided in three parts. First we give the details of the Molecular Orbitals variational calculation for the cluster. Then we describe the basis sets employed in the expansion of the MOs. Finally, we describe the several approximations that were considered in the construction of the potential field due to the external atoms in the solid.

II. 1 - The discrete variational method and HFS Halmitonian

The discrete variational method (DVM)[22] has been employed quite satisfactorily to describe electronic and magnetic properties of solids in the cluster approximation[15-17]. We give here only a brief summary of its main features and refer to the original papers for further details.

To obtain the cluster one-electron wave functions $\psi_i(\vec{r})$, an error functional is defined:

$$f_i(\vec{r}) = (H - \varepsilon_i)\psi_i(\vec{r}) \qquad (1)$$

and a linear combination of atomic orbitals (LCAO) is used to describe

each MO $\psi_i(\vec{r})$:

$$\psi_i(\vec{r}) = \sum_j \chi_j(\vec{r}) C_{ji} \tag{2}$$

where χ_j are numerical Hartree-Fock-Slater[23] atomic orbitals centered at the atomic sites. One may take advantage of the symmetry properties of the cluster and use a basis of symmetry-adapted atomic orbitals.

If a weighted average of $f_i(\vec{r})$ is minimized on a grid of sample points, the choice of weights equal to the volume per point is shown to result in secular equations formally identical to those given by the Rayleigh-Ritz variational method:

$$(\underset{\sim}{H} - \varepsilon \underset{\sim}{S})\ \underset{\sim}{C} = 0 \tag{3}$$

However, the total energy does not represent a minimum since actually the matrix elements are not integrals but sums over sample points. As the number of points increases, the sums approach the integral values and we tend towards the standard variational method.

The Halmitonian employed is a model Halmitonian, in which both Coulomb and exchange interactions are given by approximations intended to reduce the computational effort.

We have then:

$$H = -\frac{1}{2}\nabla^2 + V_{coul}(\vec{r}) + V_{x\alpha}(\vec{r}) \tag{4}$$

where

$$V_{coul}(\vec{r}) = -\sum_q \frac{Z_q}{|\vec{r}-\vec{R}_q|} + \int \frac{d\vec{r}'\,\rho(\vec{r}')}{|\vec{r}-\vec{r}'|} \cdot \qquad (5)$$

$V_{x\alpha}(\vec{r})$ is the local Slater exchange potential[23]

$$V_{x\alpha}(\vec{r}) = -3\alpha \left[(3/8\pi)\rho(\vec{r})\right]^{1/3} \qquad (6)$$

The molecular charge density is given by:

$$\rho(\vec{r}) = \sum_i n_i \psi_i^*(\vec{r})\,\psi_i(\vec{r}) \qquad (7)$$

where n_i is the occupation of MO $\psi_i(\vec{r})$. The Coulomb potential $V_{coul}(\vec{r})$ is approximated by expanding $\rho(\vec{r})$ in terms of radial atomic orbital densities centered on each nucleus[24]:

$$\rho(\vec{r}) \simeq \sum_{qn\ell} P^q_{n\ell} |R_{n\ell}(r_q)|^2 \qquad (8)$$

where $P^q_{n\ell}$ is the population of the $n\ell$ shell of atom q. We have used a variation of the standard Mulliken populations, by dividing the overlap charge in such a way that the atom with the largest eigenvector gets the larger contribution[17]. Within the approximation given by Eq. 8, the populations $P^q_{n\ell}$ define the charge destribution, and so they are iterated untill a self-consistent potential is obtained.

This model Coulomb potential was tested in several small molecules and gave satisfactory results of ionization energies, compared to Hartree-Fock or experimental values[24].

For the present calculations, all electrons of the cluster atoms were considered. In the evaluation of the integrals in Eq. 3, the statistical Diophantine method was employed[22]. For the variational calculation of CaF_2 and SrF_2, a number of points equal to 1,200 was found to be satisfactory; for BaF_2, 2,400 points were employed. All the electrons of the cluster atoms were included in the calculations. Energy eigenvalue convergence was pursued to the 3rd decimal in atomic units.

II. 2 - Choice of basis sets

LCAO - MO cluster methods use a limited, incomplete, basis set constituted of AO-like functions, centered on nuclear sites, in order to form cluster eigenfunctions. The results of an actual calculation will then depend on the choice of the set and the accuracy of the description will be related to how well the AO-like functions are able to simulate the real electronic charge density around each nucleus of the physical system.

For the present study a detailed analysis of different choices of basis sets was performed. All basis sets were obtained from atomic self-consistent HFS numerical calculations[23] for the ions F^-, Ca^{+2}, Sr^{+2} and Ba^{+2}.

A spherical potential well of depth V and radius R was added to the atomic potential V_{at}. We have then, for the potential of atom q:

$$V^q_{at}(r) = V_{at}(r) + V, \text{ for } r < R$$

or (9)

$$V^{q}_{at}(r) = V_{at}(r), \text{ for } r > R$$

This potential well, besides producing localized continuum states, can be used to reduce the radial extension of more diffuse atomic functions, decreasing the overlap between atomic orbitals centered in difer - ente nuclei; this may result in a variational basis more adequate for the description of the chemical bonds. In the present case, the basis set was defined using the following criteria: R was chosen to be the ionic radii of the ions[25], and V for F^- was made equal to the Madelung potential for an electron at the F^- site. For the cat ions, the Madelung energy is positive; however, a negative V was used to simulate the Pauli repulsion between electrons in neighbour sites, in order to get reasonable values of the energy gaps between the various bands for CaF_2. For Sr^{+2} and Ba^{+2}, this same value was used. This data is summarized in table I.

The following basis functions were obtained in the manner just described: $F^-(1s^2,2s^2,2p^6)$; $Ca^{+2}(1s^2,2s^2,2p^6,3s^2,3p^6,3d^0,4s^0,4p^0)$; $Sr^{+2}([Kr]4d^0,5s^0,5p^0)$; $Ba^{+2}([Xe]5d^0,6s^0,6p^0)$. The use of the wells with the parameters in table I produces atomic charge densities that are contracted, in the manner which is shown by X-Ray diffraction to exist around the ion sites in ionic crystals. The vacant d, s and p orbitals of the cations describe realistic conduction bands, as shall be seen later.

II. 3 - Boundary Conditions

In this section we will describe four different ways of including the field due to exterior atoms inside the finite-size cluster region, to simulate the effect of the infinite crystal.

All these boundary conditions will have as a common feature the effect of neutralizing the electrostatic charge of the ionic cluster, as it is necessary if the neutrality of the whole crystal is to be preserved in the model calculation.

a. Watson charged sphere boundary condition

Based on Watson's original idea[26], this is the simplest way of embedding in a crystal an ionic cluster of charge Q. It consists of adding to the cluster potential the potential of a uniformly changed (-Q) spherical surface which defines the so-called "Watson Sphere" and limits the cluster region. The added one-electron potential is then (in a.u.):

$$V_W(\vec{r}) = \frac{Q}{R_W} \qquad r \leq R_W$$

$$V_W(\vec{r}) = \frac{Q}{r} \qquad r \geq R_W \tag{10}$$

where R_W is the "Watson Sphere" radius. R_W is defined as the smallest radius such that the Watson Sphere surface is tangent to spheres associated to the most external ions of the cluster, the radii of

which are the ionic radii.

This boundary condition, widely used in Multiple Scattering Xα (MSXα) calculations[23,27] simulates very poorly the infinite crystal outside the cluster. The one-electron energy receives a constant contribution in the cluster region which is thus unable to reproduce real anisotropies in this region.

b. Muffin-tin boundary condition

This boundary condition, used in MSXα calculations of perfect and defective alkali-halide crystals by Yu[28] and of perfect alkaline-earth fluoride crystals by Bielschowsky and Maffeo[29], intends to incorporate some anisotropic features of the field inside the cluster, due to the external infinite crystal.

One considers the crystal space divided in three regions: region I, or "atomic region", constituted of non-overlapping spheres centered on cluster nuclei with radii proportional to the corresponding ionic radii; region II, or "interatomic region", defined by the space between the spheres of region I, inside the cluster region; region III, or "outer region", exterior to the cluster. The cluster is limited by a sphere, tangent to the most external spheres of the atomic region.

Considering now that the region of the crystal external to the cluster is simulated by an infinite set of non-overlapping spheres, centered at the equilibrium ion sites, each one enclosing a total charge equal to the charge of the ion, the boundary condition is defined by an ensemble $\{e_i; e_{IN}; e_{out}\}$ of parameters such that:

(i) e_i represents the one-electron potential energy of the interaction between an electron inside the $i^{th.}$ sphere (of volume v_i) of the atomic region, and the crystal outside the cluster; e_i is calculated, using the Madelung energies, to be the spherical average of the potential energy of the interaction between

such electron and the infinite set of non-overlapping spheres in region III.

(ii) e_{IN} represents the one-electron potential energy of the interaction between the electron, when it is placed inside the interatomic region (of volume v_{IN}), and the region of the crystal outside the cluster; e_{IN} is calculated from the volume average of the potential energy inside de cluster, giving:

$$e_{IN} = \frac{e_0 v_0 - \sum_i e_i v_i}{V_{IN}} \qquad (11)$$

where $\sum_i$ includes all spheres of the atomic region, v_0 is the volume of the "cluster sphere" and e_0 is the value of the potential energy of the interaction between an electron at the center of the cluster and the infinite set of non-overlapping spheres in Region III.

(iii) $e_{out} = \frac{e_{IN} R_c}{r}$, representing the one-electron potential energy in the outer region, is obtained by requiring continuity of the crystal potential on the surface of the cluster sphere (of radius R_c).

When the whole cluster is considered this boundary condition incorporates some of the anisotropy of the one-electron interaction with the external crystal field. Nevertheless, inside each sphere of the atomic region, and inside the interatomic region, constant values for this interaction are used, and in the outer region the interaction is made spherically symmetric.

c. Point - Charges Boundary Condition

In order to achieve a better description of anisotropic effects inside the cluster, related to the interaction between an electron and the ions outside the cluster, one replaces a finite number N of these outer ions by point charges and evaluates the resulting one-electron potential energy by

$$V_p(\vec{r}) = -\sum_{i=1}^{N} \frac{q_i}{|\vec{r}-\vec{r}_i|} \qquad (12)$$

where $\vec{r}$ is the position-vector of an electron and q_i is the point charge at the site $\vec{r}_i$, equal to the charge of the ion at that site.

To obtain a sufficiently realistic description for a reasonable value of N, the finite set of point-charges must possess the following properties:

(i) its symmetry group should contain all the elements of the symmetry group of the cluster;

(ii) to include all the ions nearest-neighbours of the cluster,

(iii) to provide a neutral system when considered together with the cluster ions;

(iv) to provide good approximate values for the Madelung energies at the ions sites inside the cluster.

The system constitued by the cluster and the set of point-charges defines a large symmetric cell which allows the reproduction of the whole crystal structure through appropriate translation operations. The value q_i of a point-charge at the surface of the cell can be evaluated according to

$$q_i = q_i'/n \qquad (13)$$

where q_i' is the charge of the ion and $\underline{n}$ is the number of cells sharing this charge. It is clear that for all "internal" point-charges the choice should be $q_i = q_i'$. This garantees the electrostatic neutrality of the system but not always property (iv). To achieve simultaneously properties (iii) and (iv) one may adjust the values q_i of subsets of symmetry-equivalent point-charges at the surface of the cell.

d. Ion - Size Boundary Condition

It is perfectly conceivable that the preceeding boundary condition provides a very good description for the effect inside the cluster due to ions outside the cluster which do not belong to the first shell near the cluster boundary. For these closest ions, ion-size effects may be relevant and the point-charges approximation may be unreasonable. In order to account for this feature it is possible to consider an electronic charge distribution around each nucleus of this shell of first neighbours, and evaluate the one-electron potential energy of the interaction (Coulomb and exchange) between a cluster electron and each finite-size ion. The proper electronic distributions may be obtained from separate self-consitent atomic calculations for the external neighbour ions[16]. The actual procedure is to sum the charge density due to these external ions to the charge density of the cluster, at each point of the integration grid described in Section II.1; this total charge density will provide the self-consistent cluster potential.

Some care must be excercised when this boundary condition is employed. In fact, previous studies of alloys and impurities in alloys[16,30] showed that is does not represent any improvement

on the point-charge boundary condition unless the Pauli Exclusion Principle is taken into account. The reason follows from the fact that the finite-size fixed charge distributions which simulate the neighbour ions define regions around the ions nuclei characterized by a very electron-attractive potential. This potential tends to "pull" cluster electrons into these regions and the Pauli Exclusion Principle is then seriously violated. If we wish to conserve the simplicity of the description of these ions it is impossible to use orbital orthogonization procedures to improve the situation. An alternative procedure[16], which preserves such simplicity, would then consist of establishing an energy penalty for the cluster electron which approaches the external neighbour ions beyond a certain distance. In the actual calculations, this is achieved as follows: if a cluster electron finds itself at position $\vec{r}$ within a radius R_F measured from the nucleus of the external ion considered, and if the one-electron total potential energy at $\vec{r}$ is less than a value V_F, then the total one-electron potential energy is made equal to V_F.

III. RESULTS AND DISCUSSION

In this section we will present and discuss the results of the present study. For CaF_2 all boundary conditions described in Section II.3 were applied, whereas for SrF_2 and BaF_2 the Watson condition was not considered.

For all crystals the cluster considered is represented in Fig. 1; it is constituted of a central F_c^- ion, the first cationic shell of four X^{+2} ions (Ca^{+2}, Sr^{+2} or Ba^{+2}) and the second shell of six external F_{ex}^- ions, having T_d local symmetry. The cluster eigenfunctions are

thus classified according to the irreducible representations of this group.

For calcium fluoride the Watson Sphere boundary condition was tested, with charge $Q_w = -1$ to neutralize the cluster, and $R_w = 7.39$a.u.

Table II shows the parameters used with the muffin-tin condition R_F, R_{X+2} and R_c are the fluorine, cation and cluster muffin-tin spheres radii, respectively, chosen as described in Section II.3. Table II also displays the values of $e_{F_c^-}$, $e_{F_{ex}^-}$, $e_{X^{+2}}$, e_{IN} and e_{out} defined in Section II.3.

The point-charge boundary condition was applied considering a finite set of 440 point charges surrounding the cluster and defining a cube containing seven anionic planes. The boundaries of this cube have only negative charges: eight charges q_v at the vertices, 60 charges q_e on the edges and 150 charges q_f on the faces. If $q_v = -1/8$, $q_e = -1/4$ and $q_f = -1/2$ ($q_{X^{+2}} = +2$ and $q_{F^-} = -1$ in the interior of the cube), one assures the eletrostatic neutrality of the system, but not good approximations for the values of the Madelung energies at the cluster ionic sites. We have then adjusted the values of q_e and q_f in order to obtain exact eletrostatic neutrality, as well as the exact value of the Madelung energy at the central F_c^- site. From the data in table III one may assess the quality of this boundary condition, by examining the percentage deviation between the exact values of the Madelung energies at the cationic and external F_{ex}^- sites and those obtained with the above approximation ($q_{e,f}^{adj}$). It is worthwhile mentioning that when these two criteria are used (eletrostatic neutrality and exact Madelung energy at the F_c^- site), the results of the calculations are very nearly independent of the finite set size; this pleasant feature

is not achieved otherwise.

The "ion-size" boundary condition was applied as described in Section II.3; 9 shells of neighbours around the cluster were considered, with spherical charge densities around each ion. This extended set was embedded in a set of point-charges, such that the total number of ions considered (cluster, exterior ions and point-charges) formed a cube of the same size as described for the point-charge boundary condition, such that the neutrality of the system is preserved and the Madelung energy of the central ion F_c^- is exact. Since the Pauli exclusion principle will be most seriously violated when a cluster electron penetrates the region around an external neighbour atom inside a sphere of radius approximatly equal to its ionic radius, R_F was made equal to the ionic radius of F^-.

The value used for V_F was 0.8Ry in all cases; for values of R_F equal to the ionic radii, we could verify that the results are quite insensitive to small variations of V_F. When V_F = 0.8Ry, good agreement with experimental values is obtained for the valence-conduction band gap.

In table IV are given the atomic values of the exchange parameter α in Eq. 6, as derived by Schwarz[31]. For the cluster calculations, a weighted mean of the atomic values was employed, and these are also given in table IV.

III. 1 - Energy levels

The one-electron energy levels of the CaF_2 cluster are shown in Fig. II for the occupied orbitals and Fig. III for the orbitals corresponding to the empty conduction band. For boundary condition

II. 3-a (Watson charged sphere), the occupied levels corresponding to Ca^{+2}(3p) and F^-(2s) are scrambled; moreover, the energy order Ca^{+2}(3p) > F^-(2s) is inverted , since the orbitals 4e, $9t_2$ and $9a_1$ have mainly F^-(2s) character, by a Mulliken-type population analysis. Another unpleasant feature of this calculation is the large gap between the energies of the F^-(2p) orbital $10t_2$, mainly localized on the central F^- ion (92%), and the rest of the F^-(2p) levels which form the valence band. The employment of boundary condition II. 3-b (muffin-tin) in calculation (b) causes the interchange of F^-(2s) and Ca^{+2}(3p) orbital energies, resulting in separate sets of levels in the order F^-(2s) < Ca^{+2}(3p). As for central ion F^-(2p) energy level ($10t_2$), its energy difference from the corresponding levels located mainly at the peripherical F^- ions decreased considerably; also significant is the change in population of $10t_2$, which is now only 70% located on the central F^-, as compared to 92% for calculation (a). The Watson Sphere model thus proves itself inadequate to the proper description of ionic crystals such as CaF_2.

Boundary conditions II. 3-c (point-charges) and II. 3-d ("ion-size") used in calculations (c) and (d) do not represent great modifications compared to the muffin-tin exterior condition; however the energy gap between the valence and conduction bands compare better with the experimental value (as shall be seen later) for these last two calculations. The $10t_2$ F^-(2p) level presents even less central ion character in calculations (c) (62%) and (d) (64%). It should be borne in mind, however, that a finite cluster calculation will always produce such inequivalences between orbitals centered mainly at central or at peripherical atoms of the cluster, since this is

an artifact of the model.

For calculation (d), which represents the most realistic model for embedding the cluster, we have, as shown in Fig. II, the upper occupied levels forming narrow bands in the order $Ca^{+2}(3s) < F^{-}(2s) < Ca^{+2}(3p) < F^{-}(2p)$, and thus retaining much of the free-ion character. As for the empty levels (Fig. III), they are all centered mainly on the cations. The first group of levels ($5t_1$ - $16t_2$) have mainly 3d character; the higher level $12a_1$ has 4s character, $17t_2$ and the group of near-lying levels $13a_1$, $18t_2$ and 8e mainly 4p. Finally, the uppermost levels $7t_1$ and $19t_2$ are mainly constituted of $Ca^{+2}(4p)$. The energy order 3d < 4s < 4p is the same as found for the Ca^{+2} free ion[32].

The energy levels schemes for SrF_2 (Figs. IV and V) and BaF_2 (Figs. VI and VII) present similar features to those of CaF_2. For these two cases the Watson Sphere model was abandoned. The same order of occupied "bands" is obtained. For calculation (c), in both cases, the main difference from CaF_2 for the empty levels which form the conduction band is the appearence of a level with mainly "s" character at the bottom of this band. For SrF_2, this is the $14a_1$ level (48% $Sr^{+2}(5s)$, 15% $Sr^{+2}(5p)$, 14% $Sr^{+2}(4d)$) and for BaF_2 the $17a_1$ level (37% $Ba^{+2}(6s)$, 24% $Ba^{+2}(6p)$, 18% $Ba^{+2}(5d)$). The "d"-like levels come next in energy, being closely spaced; finally, the group of three levels of s-p character (11e, $24t_2$, $16a_1$ of SrF_2, and $30t_2$, 14e, $19a_1$ of BaF_2) and the very antibonding levels of p character.

The charges obtained on the central anion (F_c^-), peripherical anion (F_{ex}^-) and cation (X^{+2}) for CaF_2, SrF_2 and BaF_2 are given in table V. For the Watson Sphere embedding model, the ionicity of CaF_2 is lowest. For the more realistic boundary models, all three compounds shown a very high ionicity, which is the same for CaF_2

and SrF_2, and slightly lower for BaF_2. This is probably due the fact that the larger ion Ba^{+2} favors slightly more covalent bonds.

III. 2 - Binding energies and photoelectron spectroscopy

UPS and XPS photoelectron spectra were obtained for CaF_2, SrF_2 and BaF_2[6,7,33]. The resulting binding energies may be compared to the theoretical cluster energy levels. In table VI are given the experimental results (relative to the F^-(2p) peak), and the calculated values for comparison. The calculated values are defined from the center of gravity of the corresponding set of one-electron levels in the ground state calculation.

The accuracy of this estimation could be improved, within the context of the HFS model, by taking arithmetic means of several transition-state calculation[23] eigenvalues corresponding to the ionization of the levels associated to the bands. Nevertheless, this would require a great amount of computational effort without a significant improvement of the quantitative results since the inaccuracies involved in the evaluation of ionization energies through ground-state calculation eigenvalues must be largely cancelled when energy differences are taken. Moreover, as the association between the levels obtained from cluster calculations and band levels has not a precise theoretical formulation, the increased computational effort would lack theoretical consistency.

From table VI it is seen that the accord between experiment and theory is fairly good, and that the three embedding models, muffin-tin (MT), point-charges (PC) and ion-size (IS), give similar results regarding these interband energy differences. For BaF_2, the ex-

perimental Ba^{+2}(5p) peak is split by spin-orbit coupling. This splitting[6] is as large as 2 eV, but evidently cannot be obtained theoretically at this level of approximation. The corresponding spin-orbit splitting for SrF_2 and CaF_2 is negligible.

III. 3 - Optical properties

Rubloff[5] performed a detailed study of the optical properties of CaF_2, SrF_2 and BaF_2 crystals, using synchrotron radiation as a light source to obtain reflectance spectra. The main features of these spectra are reproduced in tables VII, VIII and IX for CaF_2, SrF_2 and BaF_2 respectively. Folowing Rubloff's interpretation, the section of the spectra which is reproduced in the tables represents the valence electronic transitions, which end with the onset of the core transitions (from the cation p band), preceded by the first core exciton.

The interpretation of the optical data in our cluster model is made by associating the experimental peaks and shoulders to transitions between occupied levels from the valence band (F^-(2p)) to the empty levels of the conduction band. The energies of these transitions were taken as the energy differences between the corresponding eigenvalues in the ground state calculations. Improved transition energies may be obtained in the HFS model with self-consistent transition-state calculations in which one half electron is promoted from the lower energy orbital to the excited orbital involved[23]. This was done for the three compounds only to obtain the energy gap between valence and conduction bands (identified as the $\Gamma_{15} \rightarrow \Gamma_1$ band edge in the spectra); for the other transitions, only one-electron

$Ca^{+2}(3p)(27.0eV) > Sr^{+2}(4p)(22.9eV) > Ba^{+2}(5p)(17.5eV)$.

Our interpretation of the valence optical spectra of CaF_2 may be compared to other assignments obtained from band structure calculations; for SrF_2 and BaF_2, no such calculations are available in the literature. The recent band structure calculation[21] of Heaton and Lin for CaF_2 employes the tight-binding method with a basis set extended with single-Gaussian Bloch sums to represent Ca^{+2}(3d), (4s) and (4p) states. In their Joint Density of States analysis of the valence portion of the reflectance spectrum of Rubloff, they also assign the peaks around 14eV to $F^-(2p) \rightarrow Ca^{+2}(3d)$-type transitions; however, they do not account for the higher energy peaks (>15.5eV) in this region, which in our interpretation are due to transitions to Ca^{+2}(4s) and (4p)-type levels.

It should be mentioned that the available band structure calculations[19-21] predict for the lowest energy transition ($\Gamma_{15} \rightarrow \Gamma_1$) a Ca^{+2}(4s)-type excited state, which is not in accord with the prediction of our cluster model. In addition, certain features of band structure calculations are beyond the reach of our molecular orbitals calculations; for example, the structure in the optical spectrum that might be derived from the existence of two spatially different types of F^- ions in the CaF_2 unit cell[21,9] cannot be described by our method.

IV. CONCLUSIONS

We have performed molecular orbitals calculations for clusters representing the CaF_2, SrF_2 and BaF_2 crystals. Several different manners of taking into account the field of the external ions in the crystal have been tested. The results show that this model, when used with a reasonable scheme for embedding the cluster in the solid, gives a coherent interpretation of both photoelectron and optical data. This is particulary useful in the case of SrF_2 and BaF_2, for which band structure calculations are still lacking.

ACKNOWLEDGMENTS

One of the authors (N.C.A) acknowledges gratefully interesting discussions and suggestions from H. Manela, M.O. Mattos and P.M. Oliveira.

REFERENCES

1) S. Robin - Kandare, and J. Robin, Comptes Rendus, 262B, 1020(1966); S. Robin - Kandare and J. Robin, Comptes Rendus, 262B, 1211(1966).

2) Takeo Miyata, and Tetsuhiko Tomiki, J. Phys. Soc. Japan, 24, 954 (1968); Tetsuhiko Tomiki, and Takeo Miyata, J. Phys. Soc. Japan, 27, 658 (1969).

3) G. Stephan, Y. Le Calvez, J.C. Lemonier, and S. Robin, J. Phys. Chem. Solids, 30, 601 (1969).

4) W. Hayes, A.B. Kunz, and E.E. Koch, J. Phys. C, 4, L200 (1971).

5) G.W. Rubloff, Phys. Rev. B, 5, 662 (1972).

6) R.T. Poole, J. Szajman, R.C.G. Leckey, J.G. Jenkin, and J. Liesegang, Phys. Rev. B, 12, 5872 (1975).

7) W. Pong, C.S. Inouye, and S.K. Okada, Phys. Rev. B, 18, 4422 (1978).

8) P.E. Best, Proc. Phys. Soc., 80, 1308 (1962).

9) J. Frandon, B. Lahaye, and F. Pradal, Phys. Stat. Sol. B, 53, 565 (1972).

10) Timothy Huang, and W.H. Hamill, J. Phys. Chem. Solids, 36, 661 (1975).

11) See, for example: W.R. Hunter, and S.A. Malo, J. Phys. Chem. Solids, 30, 2739 (1969).

12) Renata Reisfeld, and Christian K. Jørgensen, "Lasers and Excited States of Rare Earths", Springer-Verlag, Berlin (1977).

13) See, for example: Ryohei Nakata, Katsuyasu Kawano, Minoru Sumita, and Eiichi Higuchi, J. Phys. Chem. Solids, 41, 1119 (1980); J.M. Baker, and R.L. Wood, J. Phys. C, 13, 4751 (1980).

14) James H. Schulman, and W. Dale Compton, "Color Centers in Solids", Pergamon Press, Oxford (1962); A.B. Lidiard, "Defects in Crystalline Solids", in "Orbital Theories of Molecules and Solids", ed. N.H. March, Oxford University Press, London (1974).

15) P.F. Walsh, and D.E. Ellis, Phys. Rev. B, 8, 5920 (1973).

16) D.E. Ellis, G.A. Benesh, and E. Byrom, Phys. Rev. B, 16, 3308 (1977)

17) Cyrus Umrigar, and D.E. Ellis, Phys. Rev. B, 21, 852 (1980).

18) Chiang Y. Yang, K.H. Johnson, D.R. Salahub, J. Kaspar, and R.P. Messmer, Phys. Rev. B, 24, 5673 (1981).

19) J.P. Albert, C. Jouanin, and C. Gout, Phys. Rev. B, 16, 925 (1977).

20) J.P. Albert, C. Jouanin, and C. Gout, Phys. Rev. B, 16, 4619 (1977).

21) Richard A. Heaton, and Chun C. Lin, Phys. Rev. B, 22, 3629 (1980).

22) D.E. Ellis and G.S. Painter, Phys. Rev. B, 2, 2887 (1970); D.E. Ellis, Int. J. Quant Chem. S, 2, 35 (1968).

23) J.C. Slater, "The self-consistent field for molecules and solids", Mc Graw-Hill, New York (1974).

24) A. Rosén, D.E. Ellis, H. Adachi, and F.W. Averill, J. Chem. Phys., 65, 3629 (1976).

25) M.P. Tosi and F.G. Fumi, J. Phys. Chem. Solids, 25, 31 (1964); J. Shanker, and S.C. Agarwall, J. Phys. Chem. Sol., 38, 91 (1977).

26) R.E. Watson, Phys. Rev., 111, 1108 (1958).

27) K.H. Johnson, J. Chem. Phys., 45, 3085 (1966); J.C. Slater and K.H. Johnson, Phys. Rev. B, 5, 844 (1972).

28) H.L. Yu, Ph. D. thesis, University of Florida (1975).

29) C.E. Bielschowsky and B. Maffeo, Phys. Stat. Solidi (in press).

30) G.A. Benesh, and D.E. Ellis, Phys. Rev. B, 24, 1603 (1981).

31) K. Schwarz, Phys. Rev. B, 5, 2466 (1972).

32) C.E. Moore, "Atomic Energy Levels", vol. 1, National Bureau of Standards (1949).

33) W. Bremser (unpublished), cited in H. Wiesner, and B. Hoenerlaye, Z. Phys., 256, 43 (1972).

FIGURE CAPTIONS

Figure I

Cluster for the variational calculations of CaF_2, SrF_2 and BaF_2.

Figure II

Self-consistent energy levels scheme for the occupied orbitals of the CaF_2 cluster. (a) corresponds to the Watson sphere boundary condition (II.3-a); (b) to the muffin-tin boundary condition (II.3-b); (c) to the point-charges boundary condition (II.3-c); (d) to the "ion-size" boundary condition (II.3-d).

Scale on the left corresponds to calculation (a); scale on the right to calculations (b), (c) and (d). All calculations were done with the same basis set, as decribed in II.2.

Figure III

Conduction levels for the CaF_2 cluster. Captions as for Fig. II.

Figure IV

Energy level scheme for the occupied orbitals of the SrF_2 cluster. (a) corresponds to the muffin-tin boundary condition (II.3-b); (b) to the point-charge boundary condition (II.3-c); (c) to the "ion-size" boundary condition (II.3-d). All calculations were done with the same basis set, as described in II.2.

Figure V

Conduction levels for the SrF_2 cluster. Captions as for Fig. IV.

Figure VI

Energy levels for the occupied orbitals of the BaF_2 cluster. (a) corresponds to the muffin-tin boundary condition (II.3-b); (b) to the point-charge condition (II.3-c); (c) to the "ion-size" boundary condition (II.3-d). All calculations were done with the same basis set, as described in II.2.

Figure VII

Conduction levels for the BaF_2 cluster. Captions as for Fig. VI.

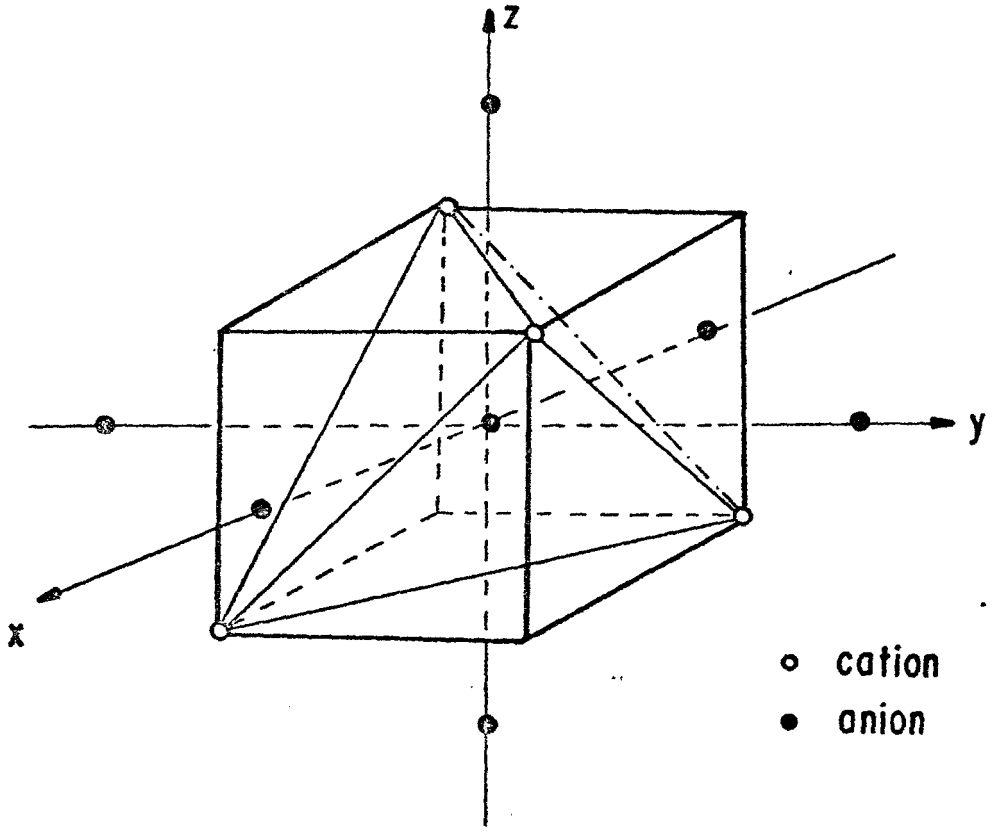

FIG. I

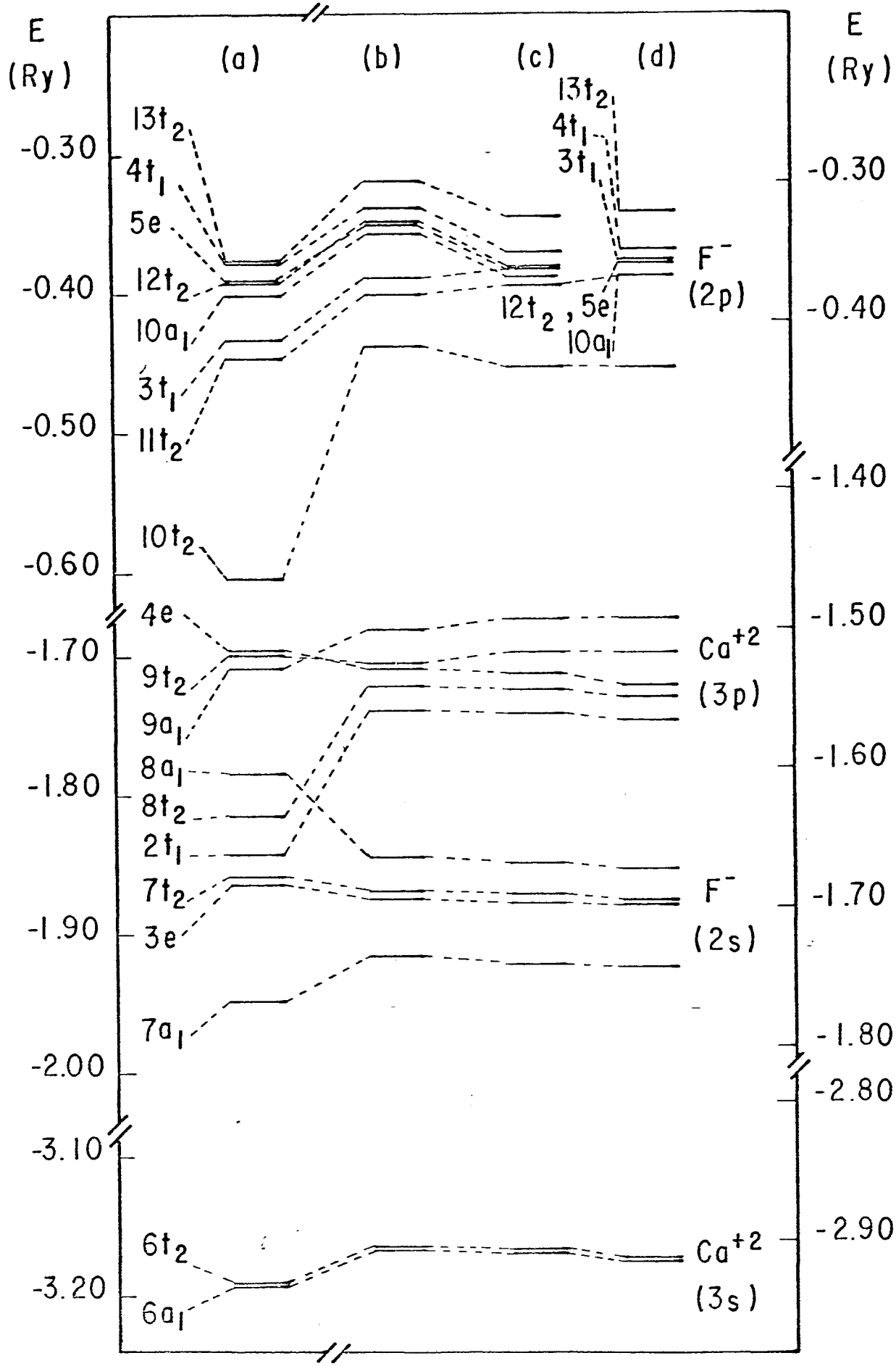
E
(Ry)
(a)
(b)
(c)
(d)
E
(Ry)
-0.30
-0.40
-0.50
-0.60
-1.70
-1.80
-1.90
-2.00
-3.10
-3.20
13t2
4t1
5e
12t2
10a1
3t1
11t2
10t2
4e
9t2
9a1
8a1
8t2
2t1
7t2
3e
7a1
6t2
6a1
13t2
4t1
3t1
12t2 , 5e
10a1
F⁻
(2p)
Ca+2
(3p)
F⁻
(2s)
Ca+2
(3s)
-0.30
-0.40
-1.40
-1.50
-1.60
-1.70
-1.80
-2.80
-2.90

FIG. II

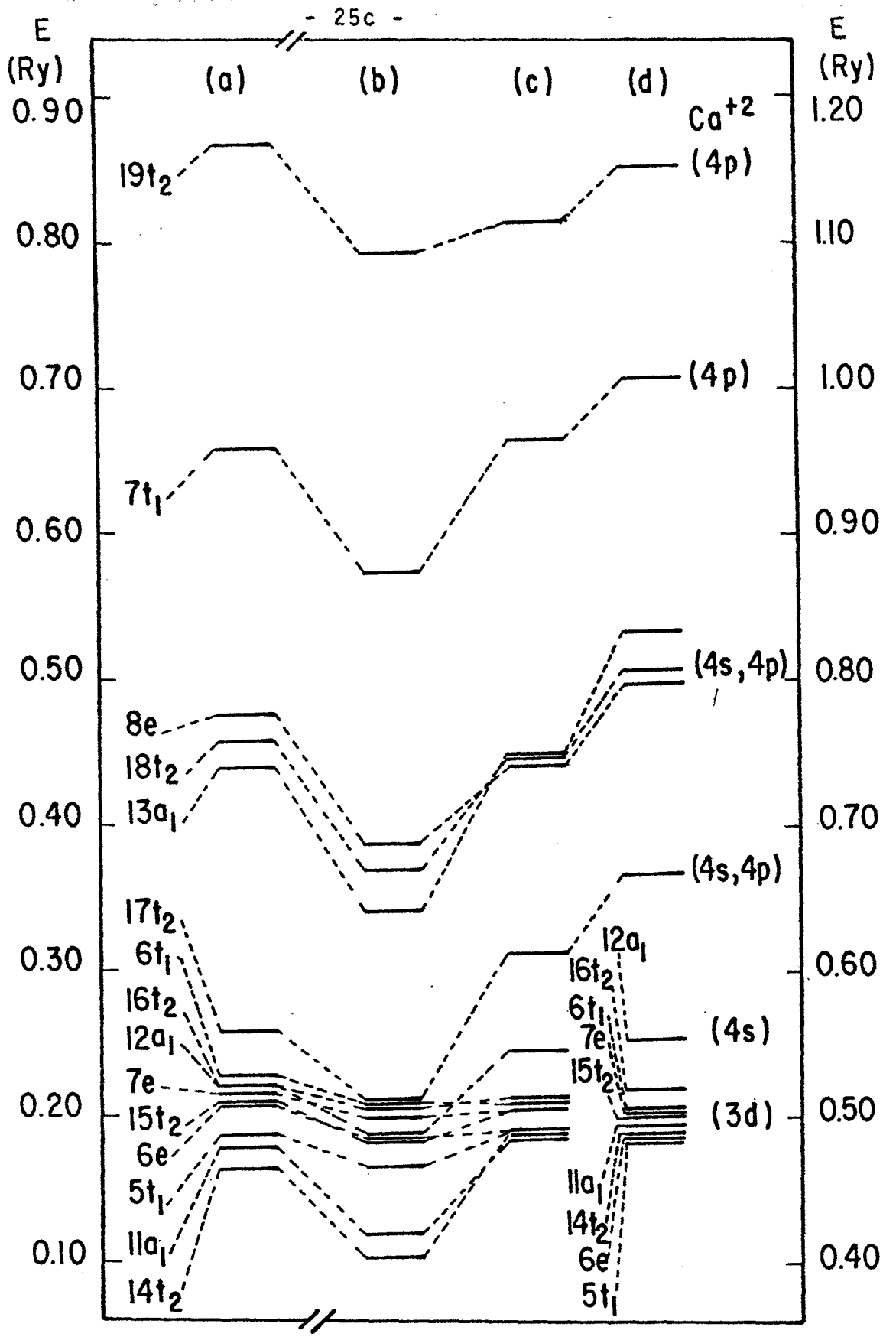
E (Ry)
(a)
(b)
(c)
(d)
Ca+2
0.90
0.80
0.70
0.60
0.50
0.40
0.30
0.20
0.10
1.20
1.10
1.00
0.90
0.80
0.70
0.60
0.50
0.40
19t2
(4p)
7t1
(4p)
8e
18t2
13a1
(4s,4p)
17t2
6t1
16t2
12a1
7e
15t2
6e
5t1
11a1
14t2
12a1
16t2
6t1
7e
15t2
(4s,4p)
(4s)
(3d)
11a1
14t2
6e
5t1

FIG. III

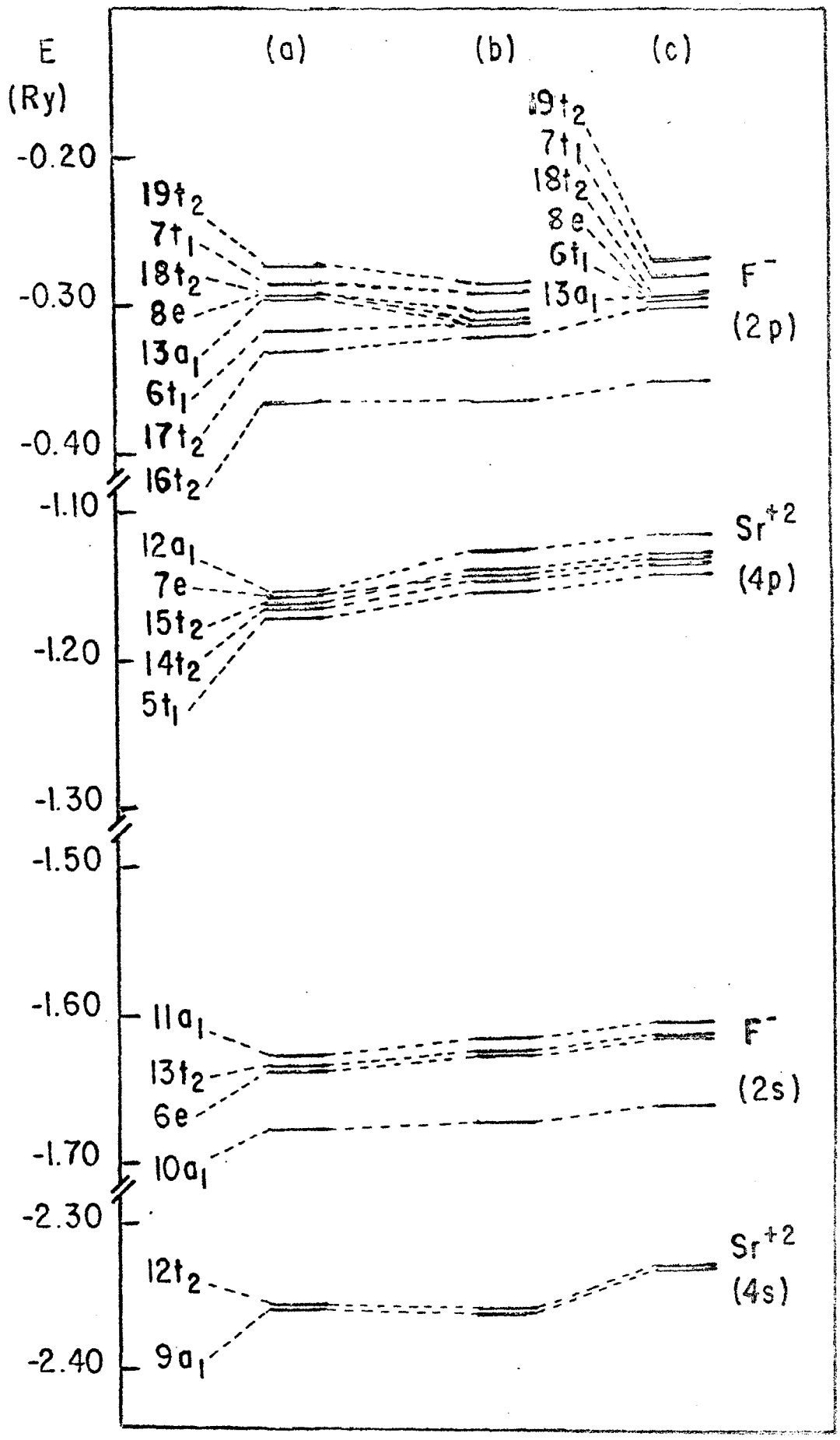
E
(Ry)
(a)
(b)
(c)
-0.20
-0.30
-0.40
-1.10
-1.20
-1.30
-1.50
-1.60
-1.70
-2.30
-2.40
19t2
7t1
18t2
8e
13a1
6t1
17t2
16t2
12a1
7e
15t2
14t2
5t1
11a1
13t2
6e
10a1
12t2
9a1
F-
(2p)
Sr+2
(4p)
F-
(2s)
Sr+2
(4s)

FIG. IV

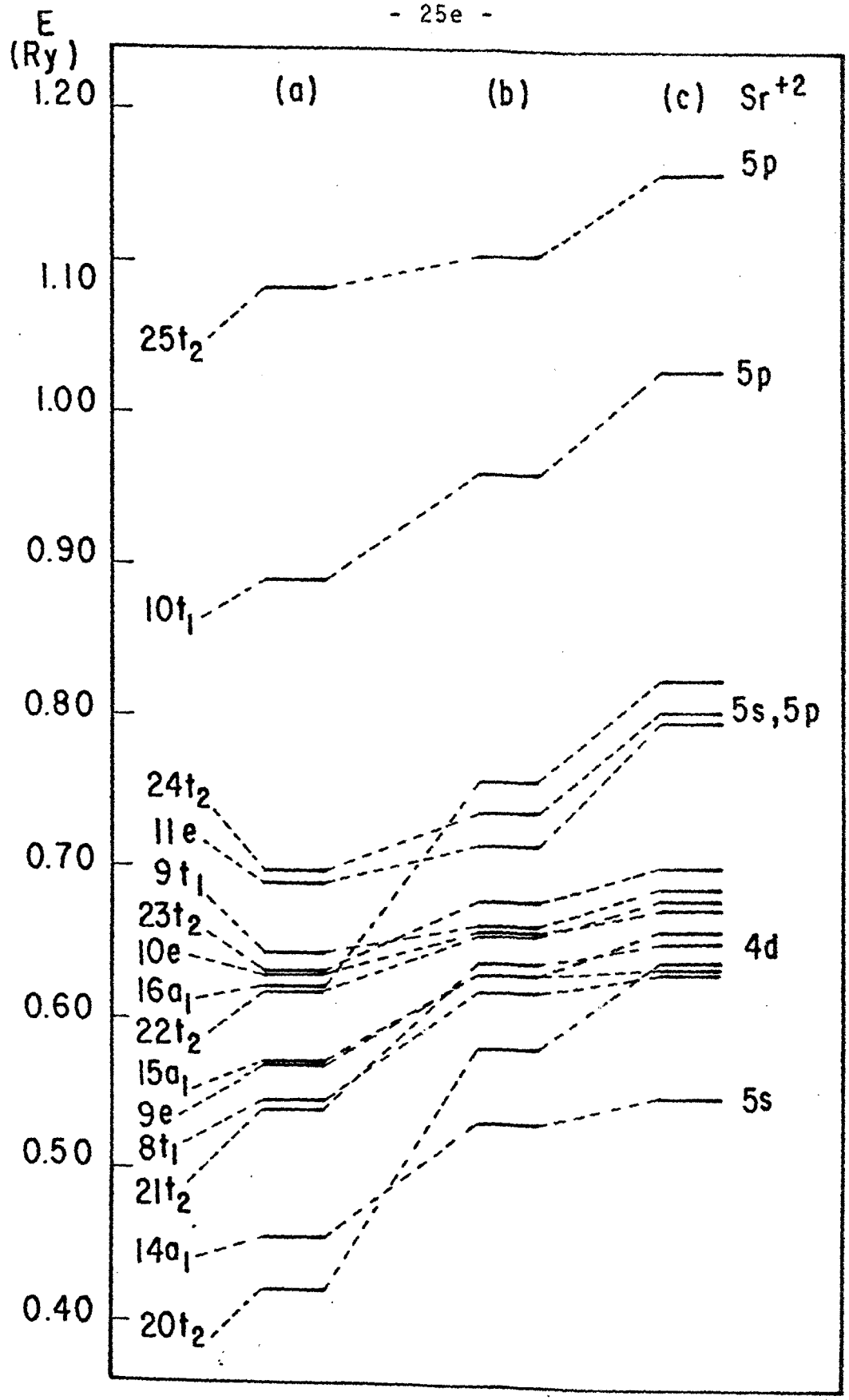
E
(Ry)
1.20
1.10
1.00
0.90
0.80
0.70
0.60
0.50
0.40
(a)
(b)
(c) Sr+2
5p
5p
5s,5p
4d
5s
25t2
10t1
24t2
11e
9t1
23t2
10e
16a1
22t2
15a1
9e
8t1
21t2
14a1
20t2

FIG. V

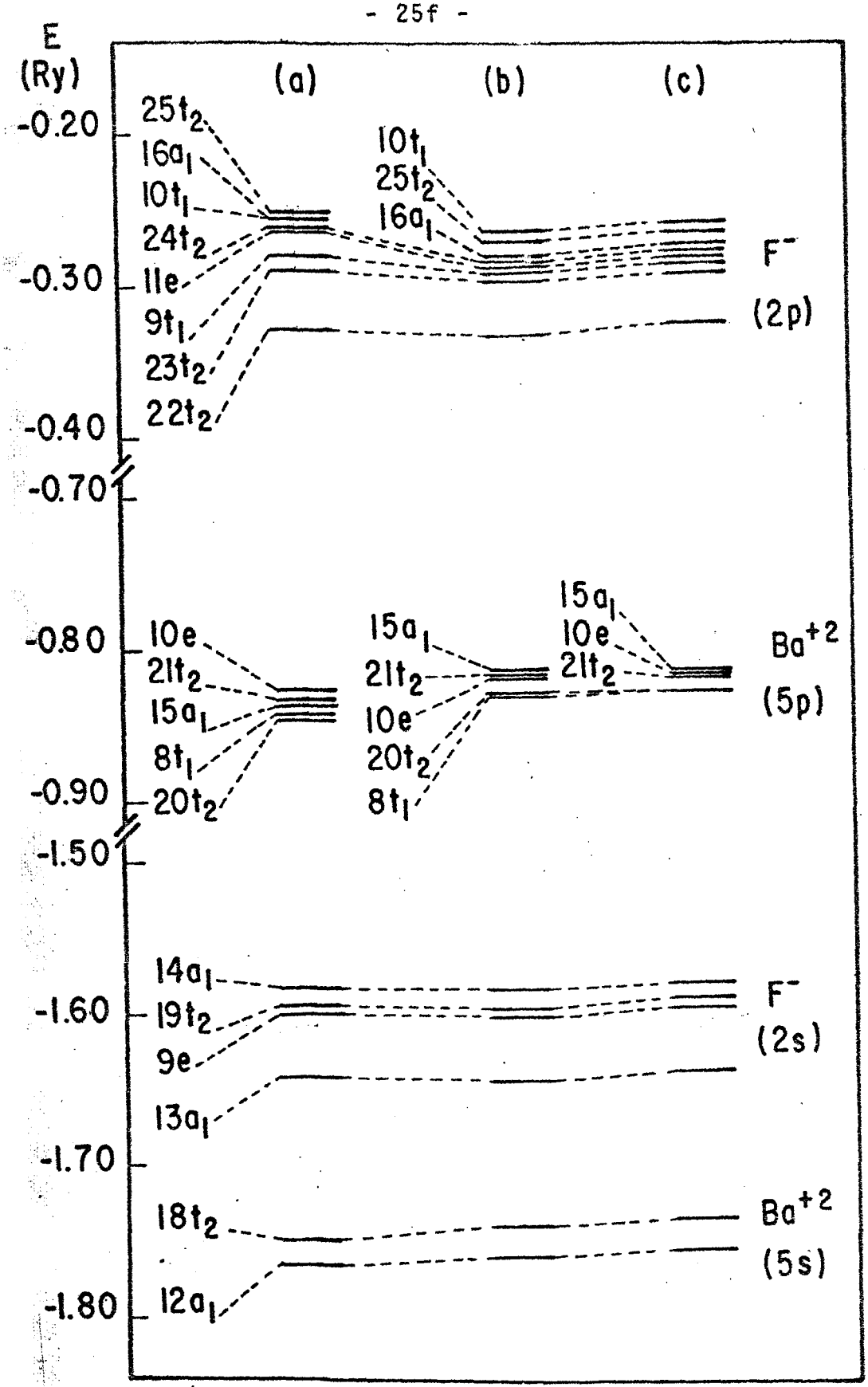
E
(Ry)
(a)
(b)
(c)
-0.20
-0.30
-0.40
-0.70
-0.80
-0.90
-1.50
-1.60
-1.70
-1.80
25t2
16a1
10t1
24t2
11e
9t1
23t2
22t2
10t1
25t2
16a1
F⁻
(2p)
15a1
10e
21t2
Ba+2
(5p)
10e
21t2
15a1
8t1
20t2
15a1
21t2
10e
20t2
8t1
14a1
19t2
9e
13a1
F⁻
(2s)
18t2
12a1
Ba+2
(5s)

FIG. VI

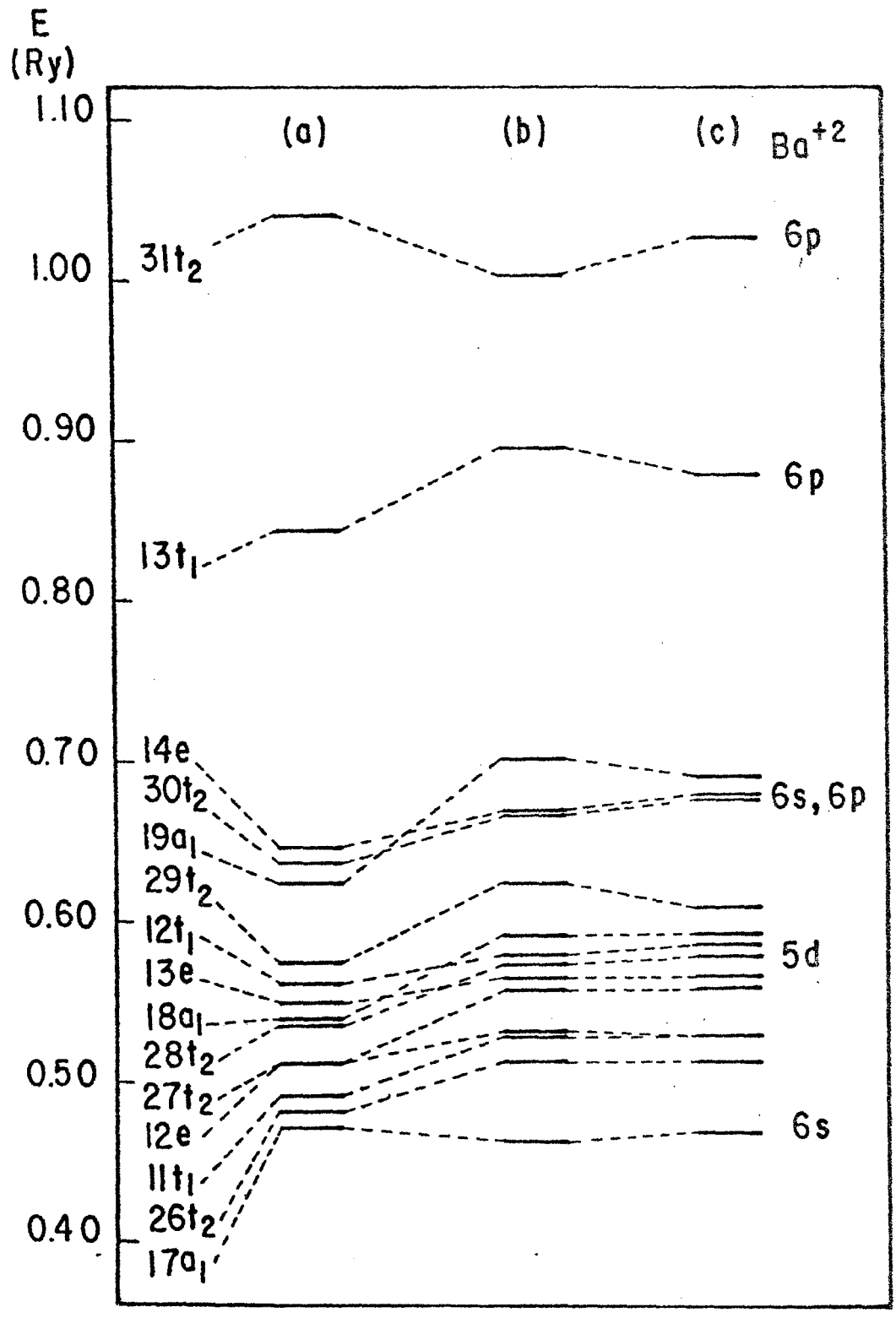
E
(Ry)
1.10
1.00
0.90
0.80
0.70
0.60
0.50
0.40
(a)
(b)
(c)
Ba+2
31t2
13t1
14e
30t2
19a1
29t2
12t1
13e
18a1
28t2
27t2
12e
11t1
26t2
17a1
6p
6p
6s, 6p
5d
6s

FIG. VII

TABLE CAPTIONS

Table I

Values of the depth V (in Ry) and radius R (in a.u) of the wells used in atomic calculations of F^-, Ca^{+2}, Sr^{+2} and Ba^{+2}.

Table II

Parameters for muffin-tin boundary condition, in a_0 and Rydberg units.

Table III

Percentage deviations between exact Madelung energies at the sites F^-_{ex} and X^{+2} of the cluster, and values calculated with a finite set of exterior ions, when adjusted ($q^{adj}_{e,f}$) and non-adjusted values of q_e and q_f are used for the central ion F^-_c.

Table IV

Values of the parameter α for $F(\Xi\alpha_F)$, Ca, Sr and $Ba(\Xi\alpha_X)$, as obtained by Schwarz[31]. Also given are the values for the cluster calculations ($\Xi\alpha_c$) (see text).

Table V

Charges on the cation (X^{+2}), central anion (F^-_c) and peripherical anion (F^-_{ex}) of CaF_2, SrF_2 and BaF_2. (WS) is Watson sphere charge condition (II.3-a); (MT) is muffin-tin boundary condition (II.3-b); (PC) is point-charges condition (II.3-c) and (IS) is ion-size boundary condition (II.3-d).

Table VI

Experimental and theoretical binding energies for CaF_2, SrF_2 and BaF_2, referred to the center of gravity of the $F^-(2p)$ band. (MT) refers to the muffin-tin embedding model (II.3-b); (PC) to the point-charges model (II.3-c); (IS) to the ion-size model (II.3-d).
a) From reference (6). b) From reference (33). c) From reference (7), measured between band thresholds. d) This value was measured from

TABLE CAPTIONS (cont...)

the middle of the two spin-orbit split 5p (Ba^{+2}) peaks.

Table VII

Optical properties of CaF_2. a) From reference (5) (reflactance spectrum). b) Transition-state calculation (see reference (23)). c) The Ca^{+2}(3p) exciton energy determines the onset of transitions from this band. Theoretical results are for the ion-size boundary condition.

Table VIII

Optical properties of SrF_2. a) From reference (5) (reflectance spectrum). b) Transition-state calculation (see reference 23)). c) The Sr^{+2}(4p) exciton energy determines the onset of transitions from this band. Theoretical results are for the ion-size boundary condition.

Table IX

Optical properties of BaF_2. a) From reference (5) (reflectance spectrum). b) Transition-state calculation (see reference (23)). c) The Ba^{+2}(5p) exciton energy determines the onset of transitions from this band. Theoretical results are for the ion-size boundary condition.

TABLE I

	CaF_2	SrF_2	BaF_2
R_{F^-}	2.25	2.25	2.25
$R_{X^{+2}}$	2.15	2.46	2.84
V_{F^-}	-0.80	-0.74	-0.70
$V_{X^{+2}}$	-1.40	-1.40	-1.40

TABLE II

	CaF_2	SrF_2	BaF_2
R_F	2.25	2.25	2.25
$R_{X^{+2}}$	2.15	2.46	2.84
R_C	7.39	7.71	8.09
$e_{F^-_C}$	0.46	0.44	0.41
$e_{F^-_{ex}}$	0.26	0.24	0.23
$e_{X^{+2}}$	0.62	0.58	0.55
e_{IN}	0.49	0.45	0.42
e_{out}	$\frac{3.62}{r}$	$\frac{3.47}{r}$	$\frac{3.40}{r}$

TABLE III

		X^{+2} site (%)	F^-_{ex} site (%)
CaF_2	$q_v = -\frac{1}{8}$ $q_e = -\frac{1}{4}$ $q_f = -\frac{1}{2}$	41	75
	$q_v = -\frac{1}{8}$ $q_e^{adj} = +0.117$ $q_f^{adj} = -0.654$	4	0
SrF_2	$q_v = -\frac{1}{8}$ $q_e = -\frac{1}{4}$ $q_f = -\frac{1}{2}$	41	78
	$q_v = -\frac{1}{8}$ $q_e^{adj} = +0.128$ $q_f^{adj} = -0.658$	0	0
BaF_2	$q_v = -\frac{1}{8}$ $q_e = -\frac{1}{4}$ $q_f = -\frac{1}{2}$	41	74
	$q_v = -\frac{1}{8}$ $q_e^{adj} = +0.122$ $q_f^{adj} = -0.655$	2	0

TABLE IV

	α_F	α_X	α_c
CaF_2	0.737	0.720	0.730
SrF_2	0.737	0.705	0.726
BaF_2	0.737	0.690	0.720

TABLE V

	CaF_2				SrF_2			BaF_2		
	(WS)	(MT)	(PC)	(IS)	(MT)	(PC)	(IS)	(MT)	(PC)	(IS)
F^-_c	-0.88	-0.91	-0.91	-0.91	-0.91	-0.91	-0.91	-0.89	-0.89	-0.88
F^-_{ex}	-0.88	-0.94	-0.95	-0.95	-0.94	-0.95	-0.95	-0.93	-0.93	-0.93
X^{+2}	+1.79	+1.88	+1.90	+1.90	+1.89	+1.90	+1.90	+1.86	+1.87	+1.87

TABLE VI

	Electronic bands	Experimental binding energies (in eV)	Calculated binding energies (eV)		
			(MT)	(PC)	(IS)
CaF_2	$F^-(2p)$	0	0	0	0
	$Ca^{+2}(3p)$	17.6 [a]	16.2	15.9	15.9
	$F^-(2s)$	22 [a]	18.2	18.1	18.2
	$Ca^{+2}(3s)$	36 [a]	34.8	34.5	34.7
SrF_2	$F^-(2p)$	0	0	0	0
	$Sr^{+2}(4p)$	12.3 [a]	11.6	11.3	11.3
	$F^-(2s)$	21.2 [b]	18.1	18.0	18.0
BaF_2	$F^-(2p)$	0	0	0	0
	$Ba^{+2}(5p)$	8.2 [a],[d] ; 7.3 [c]	7.6	7.2	7.3
	$F^-(2s)$	21.5 [b]	18.1	18.0	18.0

TABLE VII

Experimental[a]		Cluster Calculation		
energy(eV)	characteristics	energy (eV)	assignment	main characteristic of transitions
11.18	$\Gamma_{15} \rightarrow \Gamma_1$ exciton	-	-	-
12.1	$\Gamma_{15} \rightarrow \Gamma_1$ band edge	11.0 11.6[b]	$13t_2 \rightarrow 5t_1$	$2p(F^-) \rightarrow 3d(Ca^{+2})$
13.04	X_3 exciton	-	-	-
13.93	peak	11.0 -13.0	$(13t_2\text{-}10t_2) \rightarrow (5t_1\text{-}16t_2)$	$2p(F^-) \rightarrow 3d(Ca^{+2})$
14.57	peak, very temp. dep.	11.9-13.4	$(13t_2\text{-}10t_2) \rightarrow 12a_1$	$2p(F^-) \rightarrow 4s(Ca^{+2})$
15.53	peak			
16.4	shoulder	13.5-15.0	$(13t_2\text{-}10t_2) \rightarrow 17t_2$	$2p(F^-) \rightarrow 4s,4p(Ca^{+2})$
16.98	weak peak	15.2-17.2	$(13t_2\text{-}10t_2) \rightarrow (8e\text{-}13a_1)$	$2p(F^-) \rightarrow 4s,4p(Ca^{+2})$
19.12	peak	18.1-19.6	$(13t_2\text{-}10t_2) \rightarrow 7t_1$	$2p(F^-) \rightarrow 4p(Ca^{+2})$
20.35	peak			
23.3	shoulder	20.1-21.6	$(13t_2\text{-}10t_2) \rightarrow 19t_2$	$2p(F^-) \rightarrow 4p(Ca^{+2})$
25.1	$F^-(2s)$ core excitation?	-	-	-
27.7	$[Ca^{+2}(3p) \rightarrow \Gamma_1$ core exciton$]$[c]	27.0	$9a_1 \rightarrow 14t_2$	$3p(Ca^{+2}) \rightarrow 3d(Ca^{+2})$

TABLE VIII

Experimental[a]		Cluster Calculation		
energy (eV)	characteristics	energy (eV)	assignment	main characteristics of transitions
10.60	$\Gamma_{15} \rightarrow \Gamma_1$ exciton	-	-	-
11.25	$\Gamma_{15} \rightarrow \Gamma_1$ band edge	11.2	$19t_2 \rightarrow 14a_1$	$2p(F^-) \rightarrow 5s(Sr^{+2})$
		11.8[b]		
12.02	X_3 exciton	-	-	-
13.71	peak	12.3-14.3	$(19t_2\text{-}16t_2) \rightarrow (8t_1\text{-}23t_2)$	$2p(F^-) \rightarrow 4d(Sr^{+2})$
14.35	shoulder			
15.07	peak, very temp. dep.	14.5-16.0	$(19t_2\text{-}16t_2) \rightarrow (11e\rightarrow 16a_1)$	$2p(F^-) \rightarrow 5s,5p(Sr^{+2})$
15.86	peak			
16.80	peak	17.7-18.8	$(19t_2\text{-}16t_2) \rightarrow 10t_1$	$2p(F^-) \rightarrow 5p(Sr^{+2})$
19.40	peak	19.4-20.5	$(19t_2\text{-}16t_2) \rightarrow 25t_2$	$2p(F^-) \rightarrow 5p(Sr^{+2})$
22.47	$[Sr^{+2}(4p) \rightarrow \Gamma_1$ core exciton$]$[c]	22.9	$15t_2 \rightarrow 14a_1$	$4p(Sr^{+2}) \rightarrow 5s(Sr^{+2})$

TABLE IX

Experimental[a]		Cluster Calculation		
energy (eV)	Characteristics	energy (eV)	assignment	main characteristics of transitions
10.00	$\Gamma_{15} \rightarrow \Gamma_1$ exciton	-	-	-
10.57	higher exciton	-	-	-
11.0	$\Gamma_{15} \rightarrow \Gamma_1$ band edge	9.9 10.5[b]	$25t_2 \rightarrow 17a_1$	$2p(F^-) \rightarrow 6s(Ba^{+2})$
11.7	X_3 exciton	-	-	-
12.66	peak	10.6-12.8	$(25t_2\text{-}22t_2) \rightarrow (26t_2\text{-}29t_2)$	$2p(F^-) \rightarrow 5d(Ba^{+2})$
13.50	peak, very temp. dep.	12.8-13.9	$(25t_2\text{-}22t_2) \rightarrow (30t_2\text{-}19a_1)$	$2p(F^-) \rightarrow 6s,6p(Ba^{+2})$
14.34	peak			
15.5	shoulder	15.8-16.7	$(25t_2\text{-}22t_2) \rightarrow 13t_1$	$2p(F^-) \rightarrow 6p(Ba^{+2})$
16.35	weak peak			
17.10	$[Ba^{+2}(5p, j=\frac{3}{2}) \rightarrow \Gamma_1$ core exciton$]$[c]	17.5	$21t_2 \rightarrow 17a_1$	$5p(Ba^{+2}) \rightarrow 6s(Ba^{+2})$